

UAV-borne radioelement mapping

Steven van der Veeke

Deliverable for IAEA CRP project D12014



UAV-borne radioelement mapping

Towards a guideline and verification methods for
geophysical field measurements.

This publication is based on chapter 7 of the PhD thesis with the same title:

*van der Veeke, S., 2023. UAV-borne radioelement mapping: towards a
guideline and verification methods for geophysical field measurements.
University of Groningen. <https://doi.org/10.33612/diss.26126463>*

Medusa Radiometrics BV

Dr. Steven van der Veeke

Keywords: natural gamma-radiation, Monte-Carlo simulations, gamma-ray spectrometer, UAV, Medusa.

Table of Contents

Guidelines for UAV-borne radioelement mapping	3
Introduction	4
1.1 Preparation: Instrumentation	8
1.2 Preparation: Survey methodology	18
1.3 Preparation: Calibration data requirements.....	24
1.4 Survey: quality control before and during the survey	30
1.5 Post survey: Data processing	33
References	45
List of abbreviations.....	51

Guidelines for UAV-borne radioelement mapping

Introduction

The introduction of affordable heavy-duty unmanned aerial vehicles (UAVs) has led to the possibility of doing UAV-borne gamma-ray spectrometry surveys. Airborne geophysical gamma-ray studies aim to map concentrations of naturally occurring ^{40}K , ^{238}U and ^{232}Th in the environment. Historically, gamma-ray spectrometry studies characterize the geological composition of an area and aid in the search for mineral resources (Martin et al., 2015; Park and Choi, 2020; Šálek et al., 2018). More recently, this technique has been used to track down and identify artificial radioactive contamination (MacFarlane et al., 2014; Martin et al., 2016a, 2016b; Mochizuki et al., 2017; Sanada et al., 2014; Sanada and Torii, 2015; Ye et al., 2021) or as a proxy for the soil texture (Egmond et al., 2018), which is valuable input for agricultural applications.

Conventional airborne gamma-ray studies use small aeroplanes or helicopters. Ground-borne surveys are usually implemented by attaching the spectrometer to an off-road vehicle or to a backpack. The possibility of using a gamma-ray spectrometer on UAVs has led to new applications because this platform can measure over otherwise inaccessible areas at very low heights. UAVs combine the high spatial resolution of ground-based surveys with the ease of access associated with airborne surveys, albeit with a shorter range. In addition, in a UAV-borne study, the operator does not have to enter the area, thereby allowing mapping of dangerous or difficult to access areas.

However, the use of UAVs as the measurement platform for a gamma-ray survey requires a review of the methods used in conventional air- and ground-borne surveys. There are many similarities between UAV-, and conventional air- and ground-borne gamma-ray mapping studies, but there are also some obvious differences that affect the preparation, execution and data processing of a UAV-borne survey.

This document is a first attempt toward a set of '*guidelines for UAV-borne radioelement mapping*', which are intended as a manual for the implementation of gamma-ray spectrometer mapping studies using a UAV as the measurement platform. The guidelines presented in this publication have been composed by building on the information already available on the implementation of (air-borne)

gamma-ray surveys. The '*airborne gamma-ray spectrometry for natural radioelement mapping*' chapter from the '*guidelines for radioelement mapping*' manual, published by the IAEA, has been used as a starting point for this publication (Nicolet and Erdi-Krausz, 2003).

Similar to the original guidelines in the IAEA radioelement mapping manual, the guidelines presented in this publication only focus on the naturally occurring radionuclides ^{40}K , ^{238}U and ^{232}Th . Mapping naturally occurring radionuclides implies that the activity concentrations encountered are relatively low. But these concentrations vary spatially only gradually. Furthermore, in analysing the measurement, a homogeneous vertical radionuclide distribution in the soil is assumed, i.e. the concentration does not change over the first 50 cm, which is approximately the depth of view for such measurements. These assumptions are also made for the artificial radionuclide ^{137}Cs , spread in the environment due to nuclear powerplant accidents and atomic bomb testing, and therefore considered in this publication as well. These conditions for the radionuclide concentrations are significantly different from those encountered in the mapping of radioactive anomalies, for instance, when searching for lost radioactive materials. Many recommendations of these guidelines are transferable to such a situation. However, the mapping of radionuclides other than the above-listed ones is outside the scope of the current guidelines.

Another limitation in the scope of these guidelines is the choice of a UAV. This publication describes the implementation of the gamma-ray spectrometer in UAV-borne surveys but does not include an elaborate discussion about the UAV platform. First and foremost, this is because these guidelines are limited to the geophysical aspects of doing gamma-ray surveys. Secondly, technical advice on UAVs has not been included because their development is currently progressing very rapidly. The progress that has been made in the hardware, software and legislation of UAVs is vast and does not show any signs of reaching a final form yet. The latter, the regulations and law enforcements of using UAVs in public spaces, is quickly evolving and has the potential to create opportunities, but also to restrict the widespread use of UAVs. In conclusion, advice about UAVs will most likely be obsolete soon after the publication of these guidelines proposal.

The current state of the UAVs enables the use of gamma-ray spectrometers in new applications. But at the moment of writing these guidelines, there are also limitations related to the limited flying time and legislation concerning the use of UAVs. Both issues cause the spatial distance covered in a UAV-borne survey to be limited compared to conventional air-borne surveys. Until these limitations are resolved, air-borne gamma-ray surveys can operate at a much larger spatial scale than UAV-borne surveys. The current size of a typical UAV-borne survey area is more comparable to that of ground-borne or walking surveys, but with the additional benefit of not having to worry about area access over the ground. Therefore, with the current state of UAV technology and legislation, UAV-borne gamma-ray surveys are an extension of the methods available to do geophysical gamma-ray studies, as shown in Fig. 1.1.

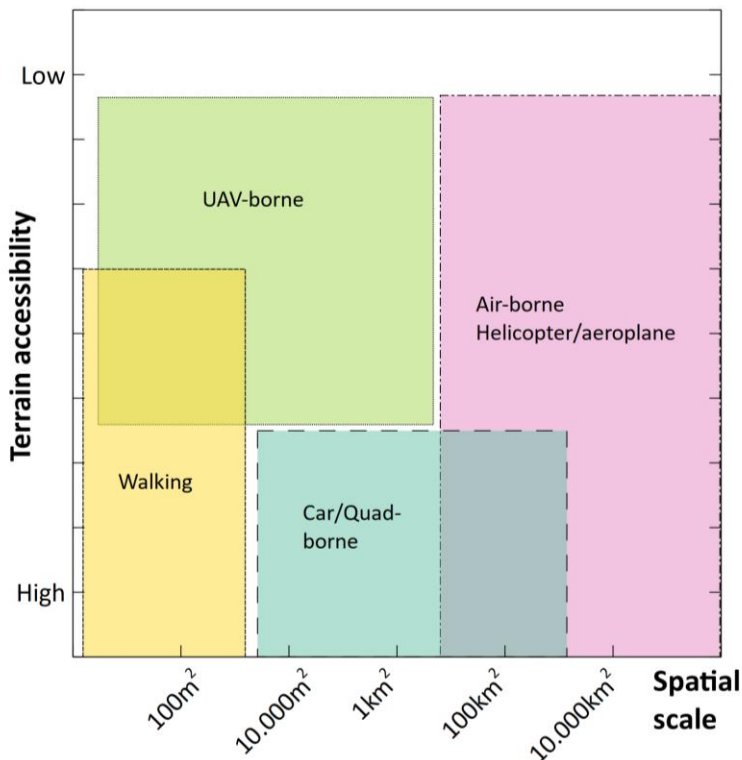


Fig. 1.1. Spatial and terrain accessibility scales for the various survey platforms commonly used in geophysical gamma-ray spectrometry studies. The x-axis shows the spatial scale in terms of the surface area that is covered in the survey. This does not include the resolution of the survey: walking, ground, and UAV-borne surveys have the possibility to capture small-scale spatial structures that cannot be captured in air-borne surveys. The figure shows that the UAV-borne studies fill the gap for low to medium scale surveys with low terrain accessibility.

Similar to the conventional survey methods, a clear survey methodology and post-survey data processing approach should be defined. This publication does this by going over the survey implementation steps in chronological order (Fig. 1.2.). These guidelines start with a discussion on the gamma-ray instrumentation and then continue with the design of a survey methodology. Subsequently, the calibration procedures required before a survey are discussed, followed by the quality control steps needed before and during the survey. Finally, the spectral data processing steps needed to acquire the radioelement concentrations are addressed. Because the use of UAVs for gamma-ray surveys is relatively new and subject to continuous development, this guidelines proposal finishes with an outlook to discuss the improvements that are expected in the coming years.

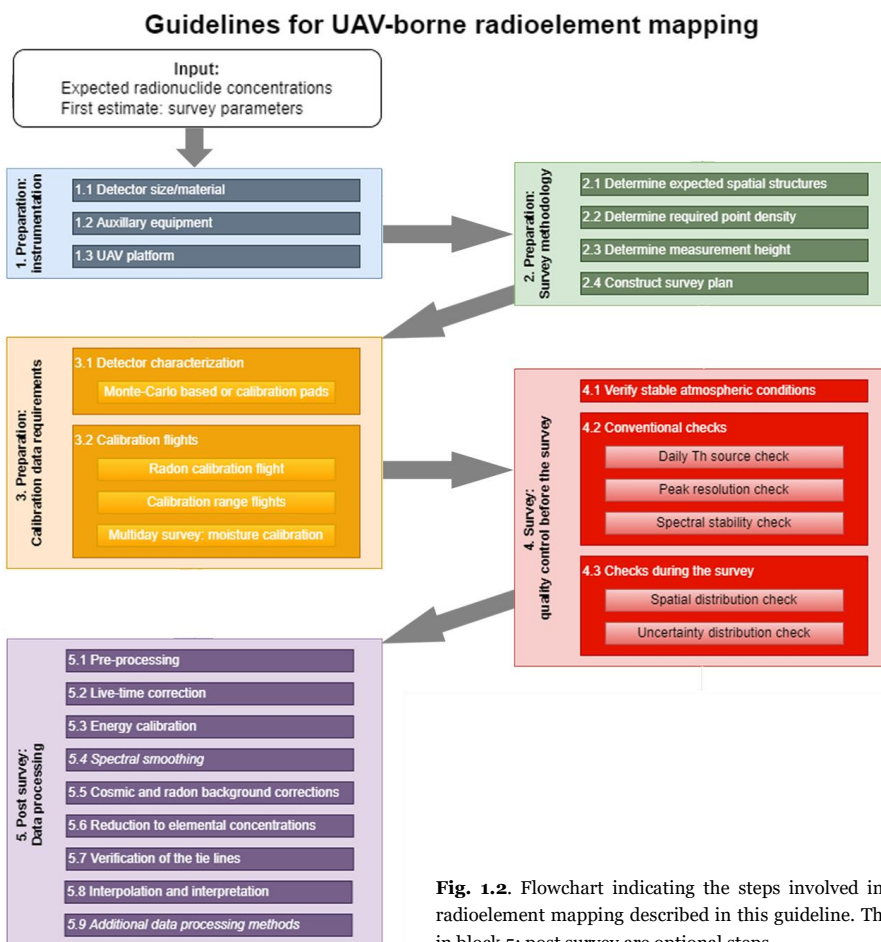


Fig. 1.2. Flowchart indicating the steps involved in UAV-borne radioelement mapping described in this guideline. The italic steps in block 5: post survey are optional steps.

1.1 Preparation: Instrumentation

Gamma-ray spectrometers detect and enable the characterization of gamma-radiation. In geophysical gamma-ray surveys, the aim is to characterize the tiny amount of radiation emitted by the naturally occurring radionuclides. Usually in these types of surveys, a spectrometer system that consists of a scintillation crystal coupled to a (silicon) photomultiplier is used. Gamma-ray photons interact with the scintillation crystal generating an electric signal that is processed by a multichannel analyser (MCA) and converted to a spectrum. The scintillation crystal can vary in shape, size and material and these parameters largely determine the recorded spectrum. The structure and intensity of this spectrum determine the accuracy of the radionuclide concentrations that can be extracted. This section describes the main factors that influence the quality of the data collected by a measurement setup when doing UAV-borne gamma-ray measurements.

A good spectrometer for UAV-borne surveys should be able to measure individual radionuclide concentrations, and the uncertainties should be sufficiently small to derive the spatial variation of the radionuclide concentrations in the survey area. Both aspects are largely determined by the scintillation crystal and measurement time and are evaluated in the survey preparation methodology. Next, the auxiliary sensors that a UAV-borne spectrometer system should include are discussed, and finally, a minimal UAV specification is described.

Compared to conventional survey setups, using a UAV as the measurement platform severely restricts the mass and volume of the payload. Maximizing the sensor mass to reach the payload limit is not necessarily the optimal approach to maximize the survey yield. There is a penalty for choosing a detector that is too large: the payload strongly influences the flight time, and every gram not needed for the measurement decreases this flying time. Therefore, in the case of UAV-borne gamma-ray spectrometry, the goal is to minimize the detector mass and volume while maintaining an acceptable quality of the data (Lee and Kim, 2019).

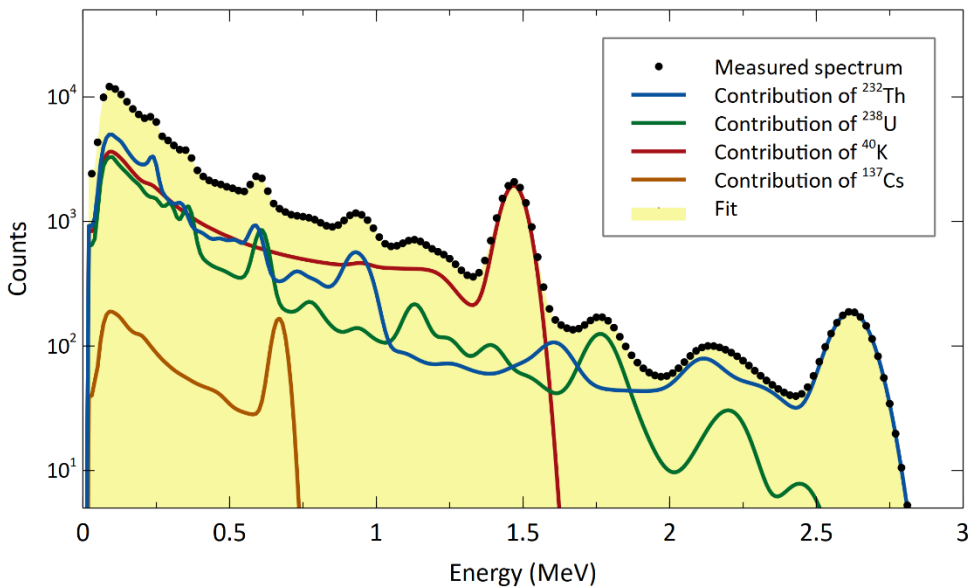


Fig. 1.3. Typical gamma-ray spectra for ⁴⁰K (red), ²³⁸U (green), ²³²Th (blue) and ¹³⁷Cs (brown) captured by a Medusa MS-1000 CsI gamma-ray spectrometer. The resolution of this spectrometer is 8.3 % at 662 keV. All four spectra have at least one prominent peak that have limited overlap with each other. The four spectra have been fitted to the measured spectrum (black dots) by using FSA, and this is described in detail in this publication, section 1.5.6.

1.1.1 Identifying radionuclides

The resolution of the detector determines its ability to distinguish radionuclides and is usually expressed by the FWHM metric at a certain energy. Gamma-rays emitted by a radionuclide have a specific energy; therefore, the resolution of the gamma-ray spectrometer should be such that the separate, individual peaks captured in the measurement can be identified. This spectral resolution is primarily determined by the scintillating crystal material and, for a small part, by the size and shape of the crystal. (Table 2.1 of van der Veeke (2023) lists some scintillation materials with their typical resolution).

In geophysical gamma-ray surveys, the concentrations of ⁴⁰K, ²³⁸U and ²³²Th and sometimes ¹³⁷Cs are measured. Fig. 1.3 shows the typical spectra of these four radionuclides measured with a spectrometer that has a resolution of 8.3 % at 662 keV. From this figure, it is clear that each spectrum has a unique peak structure, and the most prominent peaks do not overlap. Furthermore, the peaks that do overlap,

e.g. the peaks originating from ^{232}Th and ^{238}U around 0.6 MeV, can still be attributed to their respective decay chains because the overall spectra of both radionuclides are sufficiently different. When unknown peak energies need to be identified to find the radionuclide from which the gamma rays have been emitted, the overlap between peaks should be minimized. However, in geophysical measurements, it is known *a priori* what radionuclides, and their associated spectral shape, are present. Consequently, when the peak contents as a function of the radionuclide concentration are properly characterized, a relatively low resolution can be used to derive the concentrations. All crystals with their associated resolution listed in Table 2.1 of van der Veeke (2023) have been successfully used to extract radionuclide concentrations in geophysical mapping studies (Ademila et al., 2018; Jakovlevs et al., 2018; Medusa Radiometrics BV, 2020; Nilsson et al., 2014; van der Veeke et al., 2021b).

1.1.2 Uncertainty: counts

Gamma-ray spectra are expressed as counts in specific energy bins. The uncertainty in the number of counts in an energy bin follows from Poisson statistics which means that this uncertainty in the bin scales with the square root of the number of counts (A detailed description is given in the textbook composed by Gilmore (2008)). The number of counts that a gamma-ray spectrometer detects in a geophysical measurement is determined by:

The radionuclide concentration present in the area determines the photon flux hitting the detector and the count rate that is measured by it.

Table 1.1 shows a list of typical radionuclide concentrations found in geophysical measurements.

Measurement height: In geophysical measurements, the gamma rays are emitted by the soil and travel through the air before ending up in the detector. The soil and air attenuate the gamma-rays, so the gamma-ray flux decreases with height. Chapter 3 of van der Veeke (2023) or van der Veeke et al. (2021a) describe this attenuation as a function of height, and Fig 3.4 of van der Veeke (2023) shows the relative intensity of the gamma-ray flux for height ranges up to 80 m with respect to 0.80 m height.

The volume, shape, density and scintillation material: The volume the detector determines the number of gamma-rays that interact in the detector. The chemical composition and density determine the probability a gamma-ray interacts and deposits energy, and the shape determines the average path length of the gamma-rays in the crystal. To maximize the number of counts that are registered in the crystal, it should be as large as possible, have a high Z-value and density, and should be sufficiently thick so that there is a reasonable probability (> 50 %) for gamma-rays coming from the ground to interact or to be absorbed.

Table 1.1. List of typical radionuclide concentrations for various materials encountered in geophysical gamma-ray measurements. In cases where the references did not list values for all radionuclides, the missing radionuclide was estimated by using the entries from the other references listed in this table. When the reference listed multiple values from multiple samples, a value was selected that represents a typical sample.

	Potassium (⁴⁰ K Bq kg ⁻¹)	Uranium (²³⁸ U Bq kg ⁻¹)	Thorium (²³² Th Bq kg ⁻¹)
Zinc slag (Koomans et al., 2014)	400	75	20
Uranium tailings reservoir (Liu et al., 2021)	5140	20690	1210
Heavy Minerals¹ (Koomans, 2000; Meijer, 1998; Tanczos, 1996)	600	1700	6000
Calibration pads IAEA (Nicolet and Erdi-Krausz, 2003)	2504	620	512.5
Agri: Fertile soil (40 % clay) (Hebinck et al., 2007; Van der Klooster et al., 2011)	458	25	25
Agri: Bare soil (100 % sand) (Hebinck et al., 2007; Van der Klooster et al., 2011)	265	5	5
Engineering: roads (Internal documentation De Wegenscanners BV, 2021)	700	30	30
Engineering: dredging (Venema and de Meijer, 2001)	540	32	31

¹ Minerals with a density above 2.9 g cm⁻³

1.1.3 Step 1.1: Choice of detector

Material: There are many options for scintillation materials, but only a limited number materials can be grown in sufficiently large crystals at an affordable price so that they are commonly used in geophysical measurements. In this publication NaI and CsI are considered. Section 2.5.2 of Chapter 2 in van der Veeke (2023) reviews these detector materials for their use in geophysical measurements. From these two materials, CsI is the preferred choice for UAV-borne gamma-ray measurements.

Detector size (and shape): To maximize the UAV flying time, the smallest and lightest detector that still captures sufficiently accurate radionuclide concentrations in the measurement time should be selected. This accuracy is determined on the basis of the concentration uncertainty per measurement point. This value depends not only on the detector characteristics, as described above, but also on the measurement height, measurement time and radionuclide concentration of the area. A zeroth-order approximation of the relative uncertainty in radionuclide concentration per measurement point is given by:

$$\sigma_i = \frac{1}{\sqrt{C_i * I_i * t * \eta}} \times 100\% \quad (1.1)$$

in which the suffix $i = {}^{40}\text{K}, {}^{238}\text{U}, {}^{232}\text{Th}, {}^{137}\text{Cs}$. σ_i is an estimation for the uncertainty (%). C_i is the radionuclide concentration in the area of interest for the i^{th} radionuclide (Bq kg^{-1}). I_i is the number of counts registered each second by the detector for 1 Bq kg^{-1} of the i^{th} radionuclide homogenously distributed in the ground when the detector is placed at 0.80 m height. t is the time (s) for a single measurement, and η is the height dependent attenuation factor calculated from equation (3.2) of van der Veeke (2023) or extracted from Fig 3.4 in van der Veeke (2023).

The parameter I_i is specific to each detector volume, radionuclide and detector geometry. This parameter is part of the characterization of the scintillation detector, and most gamma-ray spectrometer manufacturers can provide this information, it can be calculated by using the detector specification and Monte-Carlo simulations (Van der Graaf et al., 2011), or it can be derived from a measurement in a geometry with a known radionuclide concentration. Table 1.2 list the values for I_i for a range of detectors commonly used in geophysical gamma-ray measurements.

Table 1.2. Overview of the count rates for various gamma-ray spectrometers simulated by using MCNP while the detectors were oriented with their long direction parallel to the ground. The number below the radionuclide columns represents the total number of counts in the 0.3–3 MeV energy range registered by the detector when placed 0.80 m above the ground that has a homogenous radionuclide concentration of 1 Bq kg⁻¹. The numbers in the brackets represent the number of counts in the nuclide specific energy windows (⁴⁰K = 1.37–1.57 MeV, ²³⁸U = 1.66–1.86 MeV and ²³²Th = 2.41–2.81 MeV (Nicolet and Erdi-Krausz, 2003)). Note that there is a shape induced count rate difference for the 3x9” CsI and the 90x160 mm, which have the same volume but different geometry. The geometric efficiency of scintillation detectors is known to vary and can be optimized for a specific application (Bird et al., 1993; Koomans and Limburg, 2020). I) Cylindrical detector (diameter x length). II) Rectangular prism (width x height length)

Detector	Potassium (cps Bq ⁻¹ kg)	Uranium (cps Bq ⁻¹ kg)	Thorium (cps Bq ⁻¹ kg)
Medusa MS-350 (3x3” CsI) ^I	0.077 (0.017)	0.97 (0.038)	1.10 (0.049)
Robertson Geologging Tool: 10345 (50x300 mm NaI) ^I	0.097 (0.013)	1.11 (0.029)	1.31 (0.039)
Medusa MS-700 (3x6” CsI) ^I	0.14 (0.034)	1.80 (0.079)	2.05 (0.10)
Medusa MS-1000 (3x9” CsI) ^I	0.22 (0.059)	2.76 (0.14)	3.17 (0.19)
Radiation Solutions Inc RSX-1 (4x4x16” NaI) ^{II}	0.61 (0.14)	6.71 (0.30)	8.04 (0.47)
Medusa MS-4000 (4x4x16” CsI) ^{II}	0.66 (0.19)	7.93 (0.44)	9.15 (0.66)
Exploranium GR-820 (4 seperate 4x4x16” NaI) ^{II}	1.77 (0.43)	20.5 (0.98)	24.2 (1.49)

By using equation (1.1), an estimate of the minimal detector size can be made:

Step 1: Establish a minimally acceptable uncertainty in the radionuclide concentration per measurement point. Usually, that is between 5 % and 25 % for geophysical surveys. The chosen uncertainty strongly depends on the goal of the survey and the processing steps after the radionuclide concentrations have been determined. Applications such as hotspot finding and ratio analysis typically require a lower uncertainty compared to applications where the concentrations are used to make interpolated maps and identify gradual variations in the spatial concentration distribution.

Step 2: Estimate the concentration of the radionuclides in the area that will be surveyed. This estimation should be an educated guess based on the geological information available of the area, e.g., using macroscale geological maps and tabulated values for radionuclide concentrations as presented in

Table 1.1

Step 3: Estimate the measurement height and determine the intensity reduction as described in Chapter 3 (and shown in Fig 3.4) of van der Veeke (2023) (van der Veeke et al., 2021a).

Step 4: Estimate the uncertainty for each radionuclide concentration per measured point by using equation (1.1). A measurement time is needed to estimate this uncertainty, and when this has not been determined yet, a range can be used. Measurement times in UAV-borne surveys are usually between 1 and 5 seconds. Note that the count rate values in Table 1.2 list the count rates for the 0.3–3 MeV range and in the specific windows. The count rate used in the calculation depends on the used analysis method (section 1.5.6 of this publication).

Estimating the uncertainty using the outlined stepwise approach is based on estimating the uncertainty per measurement point and can be considered the *physics* approach. In Chapter 4 of van der Veeke (2023) or van der Veeke et al. (2021b), this approach is compared with a geostatistical approach, the *geologist* approach, which uses a variogram to estimate the variation and uncertainty of the area. This publication shows that when using Kriging (Burrough et al., 2015) as the interpolation method and the variogram as the underlying model to estimate the spatial variability, the resulting interpolated maps can show a variation that would not be statistically significant based on the uncertainty estimation when using the *physics* approach of calculating the uncertainty per point. The geostatistical *geologists'* approach uses spatial information to study the dataset holistically and uses data points located close to each other to include spatial information about the concentration variation, which can result in statistically significant spatial variability for datasets of which from equation (1.1) the conclusion would be that the statistics are insufficient.

Therefore, the *physics* approach to estimate the uncertainty per point as outlined by equation (1.1) should be considered a conservative estimate when deciding the detector size. At this point in the survey preparation, a first educated guess on the detector size is made. However, this estimation should be re-evaluated after establishing the survey methodology (section 1.2 of this publication). Besides the

factors used in equation (1.1), the spatial uncertainty is dependent on the movement speed of the measurement platform and the expected spatial variation of the area. These parameters are discussed in the next section. Establishing the detector size is an iterative process in which the various aspects that influence the measured radionuclide concentration and uncertainty are weighted to optimize the measurement configuration for the survey.

Detector specifications for radon corrections: In or near areas with high uranium concentrations, the influence of atmospheric radon can perturb the determination of the uranium concentration in the ground. The contribution of radon decay in the atmosphere to the data should be subtracted from the measurements. In Chapter 5 of van der Veeke (2023), two methods to extract the contribution of radon decay to the data are described: the first method relies on measurements in the field, and the second on a change in the detector design (split detector). In areas with a high probability of perturbations due to atmospheric radon, the split detector design might be the most effective implementation of radon identification.

1.1.4 Step 1.2: Auxiliary equipment

Geophysical gamma-ray measurements that map the absolute radionuclide concentration of an area need additional sensor readings. The minimal requirements are a GPS (or more generally a GNSS), a height measurement, preferable by an absolute height sensor such as a laser altimeter (LiDAR), and atmospheric pressure and temperature sensors. Section 1.5 of this publication describes the use of these sensor readings in the post-processing step of the survey.

When using UAVs, the measurement height can be an ambiguous parameter: it can mean a certain height with respect to the take-off point (absolute height) or at a certain height above the ground (constant height or ‘drape mode’). Variations in the spatial topology are ubiquitous and the radiation intensity strongly depends on the actual height above the ground, but this can be accounted for (Chapter 3 of van der Veeke (2023) or van der Veeke et al. (2021a)). An effective height that includes

atmospheric pressure and temperature should be used. Not using the correct atmospheric parameters can lead to intensity differences of up to 10 % (Chapter 6, section 6.2.2 of van der Veeke (2023)). If the survey contains measurements at different heights, this correction is crucial to map the absolute radionuclide concentration in the ground correctly. However, this height correction only accommodates the change in intensity and not the change in footprint, which is also strongly influenced by the measurement height. If a survey is flown at several heights, the interpretation and interpolation of the results are not straightforward because the measurements have different footprints. Therefore, it is advised to adopt a survey plan with a constant height above the ground of the measurement platform, and the measurement of elevation should reflect the absolute separation between the ground and the spectrometer. Usually the area within the footprint is not completely flat, and as a rule of thumb, variations of 5 m within the footprint are acceptable (van der Veeke et al., 2021a).

The GPS sensor that adds the spatial position of the sensor to the spectral data is as crucial as the spectrometer. A standard GPS that outputs the position at the same rate as the spectrometer is usually sufficient for mapping radionuclides. Standard GPS has an accuracy of 1.5 m circular error probable (CEP (Liu et al., 2018)), which is small compared to the footprint of spectral measurements. However, if higher accuracy is needed, as can be the case for close to ground high-resolution measurements, a Real-Time Kinematic GPS (RTK GPS) can be used with an accuracy down to 1-centimetre CEP (e.g. Trimble Inc. (2022) or uBlox (2021)).

1.2 Preparation: Survey methodology

A geophysical gamma-ray survey aims to characterise the spatial radionuclide concentrations of ^{40}K , ^{238}U and ^{232}Th in an area. In areas where ^{137}Cs is present due to anthropogenic activity, this radionuclide can be included in the characterization aim of the survey. The spatial characterization is achieved by moving a gamma-ray spectrometer over the area. Ideally, the gamma-ray survey covers the whole surface of the area. A large measurement footprint of the gamma-ray spectrometer enables this requirement without having to interpolate the concentration between measurement points. However, independent of the size of the footprint, no spatial variation within this footprint can be detected when a single measurement is used.

If footprints of different measurements overlap, structure within the footprint can be determined to a degree dependent on the amount of overlap.

The height, speed, frequency, and spatial measurement grid define a geophysical gamma-ray survey. Usually, this grid is a regular spaced spatial pattern that covers the whole area by flying parallel lines that have a certain spacing. However, an area might not have a regular shape, and obstacles may make it impossible to fly a regularly spaced grid. The UAV platform offers the opportunity of implementing complex, computer-driven flight paths that include stationary points to collect extra detailed information, and this has led to the investigation of flight path optimization to cover all the areas of a survey (Cabreira et al., 2019; Zhang et al., 2018). Although it is expected that with the implementation of autonomous UAV platforms, computer-driven survey planning will become an increasingly effective tool in survey optimization, at the moment of writing, UAV surveys are generally flown by an operator. Therefore, a conventional regular spaced spatial pattern with parallel lines is assumed in the following steps that describe the design of a survey methodology. The steps described in the section below are proposed to construct a substantiated measurement plan in which the height, speed and measurement frequency are optimized.

Note that the steps below describe a theoretical approach to designing the optimal survey plan. In practice, there are usually limitations to the survey. Available funds, time, or other restrictions complicate implementing the optimal theoretical survey plan. All these practical aspects of determining the survey plan are considered in step 2.4 (section 1.2.4) and are preceded by the determination of the optimal survey plan:

1.2.1 Step 2.1: Determine the spatial structures that need to be characterized.

The size of the spatial structures that need to be characterized in a survey depends on the goal of the survey. Geological structures usually have slowly varying spatial radionuclide distributions, meaning that measurable concentration variation occurs over distances of 50 m or more (Billings et al., 2003; Knotters, 2015; Qassas et al., 2020; Taha et al., 2021). Agricultural applications aim to characterize spatial structures present in the field that are similar in size as the spatial structures present in geological applications, and with long-term cultivation, the spatial mixing of the

top layer increases the equalization of spatial structures even further. Other examples of gamma-ray surveys aim to characterize the sand and clay distribution (Egmond et al., 2018; Van der Klooster et al., 2011), sludge levels (Koomans et al., 2019; Koomans, 2000) or contamination in an area (Förstner et al., 2016; Koomans et al., 2014; Söderström and Eriksson, 2013; Van der Graaf et al., 2007). These applications can have spatial extents down to the ten-meter scale. The extent of the spatial structures that need to be characterized in the survey is used in the next steps as an upper limit for determining the movement speed, measurement frequency and flying height.

1.2.2 Step 2.2: Determine the optimal point density (speed and measurement frequency)

The Nyquist-Shannon sampling theorem (Shannon, 1949) can be used to determine the minimum sampling density; this is explained in detail in Appendix F of van der Veeke (2023). Spatial structures should be sampled at an interval of at most half the size of the spatial scale of the variations to be detected. This sample interval results in a distance between consecutive measurement points. By using the effective measurement frequency (see Appendix F of van der Veeke (2023)), it is possible to calculate the maximum movement speed and parallel line spacing of the survey. This distance should be used between the lines flown in the survey to create an evenly spaced grid.

1.2.3 Step 2.3: Determine the optimal measurement height (footprint)

Even if a gamma-ray spectrometer is not moving and is placed at a stationary position, the measurement does not reflect the radionuclide concentrations at the point coordinate. The recorded spectrum reflects the average radionuclide concentrations within the measurement footprint. The measurement footprint of the gamma-ray spectrometer as a function of heights is described in Chapter 3 of van der Veeke (2023) or van der Veeke et al. (2021a), and Appendix E of van der Veeke (2023) shows the estimation for the 65 %, 95 % and 99 % upper limits of the footprint radius for a selection of commonly used heights in UAV-borne measurements. Variations in radionuclide concentrations within the footprint perpendicular to the measurement direction cannot be detected, and in the direction of the measurement can only be roughly estimated. In addition, a moving measurement will result in an elongation of the footprint. Both these concepts are

described in detail in Appendix G of van der Veeke (2023). To summarize the information in this appendix; the footprint has two implications:

1. Regression to the mean within the footprint region: The resulting radionuclide concentration of the measurement is a spatially weighted average of the radionuclide concentration within this footprint (as schematically shown in Fig. G.2 and Fig. G.3 in Appendix G of van der Veeke (2023)). The surrounding concentration influences a local anomaly located within the size of the footprint. Therefore, in a measurement, (relative) hot- and cold-spots are smoothed by the surrounding radionuclide concentration.

2. Maximal spatial resolution: Spatial radionuclide distributions with variations at a scale that falls within the footprint cannot be captured (as schematically shown in Fig G.1 in Appendix G of van der Veeke (2023)). Therefore, the survey requirements (spatial resolution) dictate the maximum footprint, which translates to the maximum measurement height.

The measurement height and thus the size of the footprint are closely related to the sampling density described in the previous step. The Nyquist-Shannon theorem, described in step 2.2 (and Appendix F of van der Veeke (2023)), can be used to estimate the maximal spatial resolution. A sampling density of twice the spatial frequency of the variations to be detected present means that the footprint should not extend beyond half of the length of the smallest structure. However, the footprint does not have a hard cut-off in spatial extent, and therefore this requirement is not a strict requirement and a mere approximation. Consequently, the following rule of thumb could be used as a first order approximation of the concentration at a specific point: at least 65 % of the radiation that originates from an area half the size of the smallest spatial structure needs to be captured in a single measurement used to derive the radionuclide concentration.

1.2.4 Step 2.4: Construct a survey plan

Step 2.2 dictates the optimal grid spacing and the speed of the measurement platform. Usually, the grid is supplemented with tie-lines used for validation of the measurement. These tie-lines are flown at the same height, perpendicular to the measurement grid and typically have a line-spacing 5 to 10 times the main line-spacing (Nicolet and Erdi-Krausz, 2003). Step 2.3 estimates the footprint and

recommends the measurement height. The information given in these two steps fully specifies the theoretical measurement configuration. However, in practice, it is often found that there are constraints that prevent the implementation of the optimal survey plan. These constraints include field conditions (expected weather, spatial design of the area and obstacles such as trees and buildings), available time, available propellant, available funds for implementing the survey, and all other practicalities that can constrain the implementation of the ideal survey. These restrictions can result in a larger grid spacing, greater movement speed or a larger fly height. In the case of a deviation from the optimal survey plan, the consequences for the ability to fulfil the survey goal should be considered using steps 2.2 and 2.3. If the survey cannot resolve the spatial structures defined in step 2.1, either the required minimal spatial structure should be increased, or the survey height, speed or grid spacing should be adapted. Both approaches require an evaluation of the survey goal and discussion with the research stakeholders. Adaptation of the survey plan is an iterative process in which steps 2.1 through 2.4 should be re-evaluated before ending up with a final survey plan.

When a final survey plan has been determined, it has to be translated into a practical implementation in the form of a flight path. In the case of UAVs, there are many (commercial) software packages available that can be used to plan the survey. Fig. 1.4 shows a typical example of a measurement plan and the associated UAV mission. In addition to the parameters described in this section, this plan should also include a flight plan for the UAV. If the survey cannot be flown with a single battery, one or multiple take-off points and a strategy for changing the batteries should be included in this plan. At this point in the preparation of the gamma-ray survey, the measurement hardware and survey plan have been defined, but before the UAV can take off and start the survey, several preparatory steps have to be taken to ensure the quality of the collected data. These preparatory steps are outlined in the next sections.



Fig. 1.4. A typical view of the software used to prepare and execute a UAV survey. This screenshot shows the software package UgCS, version 4.6.520 (UgCS, 2022). An evenly spaced grid is used in this UAV survey. Flight planned, executed and screenshot generated by vliegend.nl (Vliegend.nl, 2022).

1.3 Preparation: Calibration data requirements

Calibration of the gamma-ray spectrometer is essential for determining absolute radionuclide concentrations in the ground. This section describes the steps that should be taken before the survey takes place to ensure the quality of the collected data and to enable the calculation of absolute radionuclide concentrations from the survey data.

1.3.1 Step 3.1: Detector characterizations

In the data processing step, the acquired spectrum is translated to radionuclide concentrations. Thus, it is necessary to obtain the relation between the peaks, and their intensity, present in the spectrum and the radionuclide concentration in the ground. General approximations can be made based on the crystal volume and shape, but the exact translation of counts to radionuclide concentration is unique for each detector due to the crystal, housing and electronic configuration. Therefore, the gamma-ray spectrometer has to be calibrated.

This calibration is done by measuring with the spectrometer in a well-defined configuration with-known concentrations of the naturally occurring radionuclides. The goal of the measurement is to characterize the response of the detector to an activity of 1 Bq kg^{-1} . This characterization can be done by using a geometry with known concentrations, such as described by Van der Graaf et al. (2011), or by measuring on $1 \times 1 \times 0.3 \text{ m}$ concrete calibration pads that contain known concentrations of ^{40}K , ^{238}U and ^{232}Th (Loeborg, 1984; Nicolet and Erdi-Krausz, 2003).

Using calibration pads for detector characterization is an empirical approach based entirely on measurements and was the most common calibration method until the early 2000s. By doing measurements on several calibration pads that primarily contain a single radionuclide (^{40}K , ^{238}U and ^{232}Th), the spectrometer's response for each radionuclide is derived independently. The effect of attenuation due to height is simulated by placing plywood panels between the calibration pads and the detector. This method has a couple of caveats: first, you need to have access to, or construct these calibration pads²; secondly, the pad is much smaller in size and

² Instructions how to build these pads can be found in Loeborg (1984). It should be noted that these pads are heavy and as a result are not easily transported.

thinner than the footprint (Chapter 3 of van der Veeke (2023) or van der Veeke et al. (2021a)). Third, the pads never contain a single radionuclide, there is always some presence of the other naturally occurring radionuclides in the pad. And finally, it has been shown for a number of pads that are used for calibration measurements that the concentration within this pads can deviate up to 30 % from the mean value (Grasty and Shives, 1997).

Since the introduction of more powerful computers, there is an alternative to the empirical methods: Monte-Carlo simulations of radiation transport are able to calculate the response of a spectrometer (Van der Graaf et al., 2011). Since the beginning of the 2000s, computers have been powerful enough to calculate the detectors' response efficiently, and with the ongoing increase in computer power, the results of these calculations continue to improve enormously. Van der Graaf et al. (2011) describe how a gamma-ray spectrometer can be calibrated by using Monte-Carlo simulations. Measurement in a geometry with known radionuclide concentrations is still necessary to characterize the crystal and electronic characteristics of the detector. However, when these have been determined, this calibration can be used for any measurement geometry: flatbed (as often assumed in air- and ground-borne measurements), borehole or other complex geometries. For a different geometry, only a new simulation needs to be performed. The characterization of the spectrometer in the calibration setup has to be done only once. This Monte-Carlo approach allows the determination of the geometry-independent detector parameters, which cannot be isolated and transferred to a different geometry when using the empirical approach.

Both the empirical and the Monte-Carlo-based calibration serve to characterize the gamma-ray spectrometer and have the purpose of deriving radionuclide concentrations in the ground. Calibration of spectrometers should be done periodically and when equipment modifications to the detector have been made. The recommended calibration interval ranges from one to five years. The one-year interval is recommended for airborne gamma-ray spectrometers that are calibrated using the calibration pads (Grasty and Minty, 1995). Modern spectrometers calibrated using the Monte-Carlo approach have shown that there is no observable change in the detector characteristics over the time period of a year (Medusa Radiometrics BV, 2020). Therefore it is recommended to calibrate the detector

either a) when the detector does not pass the quality checks described in section 1.4 of this publication, b) when the detector geometry has changed, or c) at least every five years (Medusa Radiometrics BV, 2020).

1.3.2 Step 3.2: Calibration flights

Conventional airborne radioelement mapping prescribes the implementation of various calibration flights to correct the recorded radiometric data. These flights are time-consuming, sometimes difficult to implement and focus on large-scale surveys. For UAV-borne radioelement mapping, these calibration flights can be omitted or strongly reduced in measurement time. The paragraphs below review the calibration flights prescribed for conventional airborne gamma-ray spectrometry and propose an implementation for UAV-borne gamma-ray measurements.

High altitude background calibration flights should be done by flying at several high altitudes (range 1–3.5 km) above a large body of water in the absence of atmospheric radon (Nicolet and Erdi-Krausz, 2003). This flight is to establish the background concentrations embedded in the measurement platform and to establish the contribution of cosmic-ray induced counts as a function of height. These flights are difficult or impossible to implement when using UAVs because of flight height restrictions. In UAV-borne surveys, a carrier background flight is not needed because the amount of radioactive elements embedded in the UAV can usually be neglected. Therefore no carrier background corrections have to be applied.

Cosmic rays are all the particles that bombard the earth and have been formed in outer space. The dose rate of cosmic radiation at sea level is of the same magnitude of the terrestrial gamma dose rate. The annual dose rate of cosmic radiation depends on the position on earth and the solar cycle and is estimated to be 31 nGy h^{-1} ($\pm 10 \%$), whereas the global average terrestrial gamma-dose rate is estimated at 59 nGy h^{-1} (United Nations Scientific Committee, 2000). This cosmic dose rate increases with height and doubles every 2000 m (Nicolet and Erdi-Krausz, 2003). Cosmic radiation consists mainly of protons and alpha particles with energies up to 10^{20} eV (A. Aab et al., 2000; United Nations Scientific Committee, 2000). These high-energy cosmic particles interact with atoms in the earth's atmosphere resulting in a cascade of lower energy particles, which in turn can have excited nuclei that may emit gamma radiation during their decay. These photons are generated throughout the

atmosphere, and the gamma-rays that reach the earth's surface make up the cosmic background in geophysical measurements. The resulting spectral shape is constant with height and has little structure except for a clear peak at 511 keV due to positron annihilation (Share, 1999). The remainder of the spectrum can be modelled by a power-law function (Letaw et al., 1989; Stenberg and Olsson, 1968).

The goal of the high-altitude calibration flights is to measure the cosmic spectrum. At altitudes above 1 km, the terrestrial gamma-rays are almost completely absent, and the measured spectrum is the result of the carrier background and cosmic radiation. By flying at several altitudes, the carrier background (static component) can be separated from the cosmic component (height dependent). The cosmic spectrum can be used to correct spectra recorded at lower heights by measuring a cosmic channel, in which the counts above 3 MeV are collected. The number of counts collected in the cosmic channel is used to scale the cosmic spectrum before subtracting it from the measured spectrum (Nicolet and Erdi-Krausz, 2003).

A feasible alternative to the high-altitude flights for UAV-borne measurements to establish a cosmic spectrum is a background measurement over a body of water of at least 1 m in depth when it has been verified that no radon is present (Minty, 1998; Nicolet and Erdi-Krausz, 2003). The detector should be shielded from the shore by a separation of at least 200 m, the material of which the boat is made should contain no radionuclides, and the measurement should be done over fresh water. The measured spectrum consists of the internal spectrometer background and the cosmic ray contribution. By assuming the internal background is negligible³, this measurement can be used as a cosmic spectrum that scales linearly with the cosmic channel. Alternatively, similarly to the generation of standard spectra, Monte-Carlo simulations can be used to simulate a cosmic spectrum, e.g. by using the cosmic-source option in MCNP (McKinney et al., 2012). To this date, the latter approach remains to be verified by experiments.

Radon calibration flights measure the incoming gamma-rays when flying over a large body of water while being sufficiently separated from the shore. Since fresh water does not emit any radiation, only radon in the air and cosmic radiation from

³ This is not always a valid assumption for detectors that are not made of CsI or NaI. E.g. Cheng et al., 2020; Radulescu et al., 2007, or when the detectors have been activated through neutron capture.

above is measured. A prerequisite for this calibration flight is the presence of such a body of water near the survey area. For UAV-borne measurements, the extents of the survey are much smaller than conventional airborne measurements, and often no such body of water is present within the flying range of the UAV. Therefore, this type of calibration measurement is not feasible for most UAV-borne surveys. However, the presence of radon will still influence UAV-borne radiometric measurements. Chapter 5 of van der Veeke (2023) reviews the current radon correction methods and their applicability for UAV-borne measurements. It is concluded that the current radon methods (Minty, 1998; Nicolet and Erdi-Krausz, 2003) can not be applied to UAV-borne measurements.

However, two new possibilities to correct for atmospheric radon are proposed. One method is based on a change in the geometry of the scintillation crystal. The other method can be implemented with any detector-UAV configuration and requires stationary measurements at several heights. This last method is based on the assumption that the air is homogeneously filled with radon. On the ground, the detector measures the radiation related to radon decay coming from an infinite half sphere, and when moving away from the ground to larger heights, this geometry gradually shifts to an infinite full sphere geometry. By measuring the count rate as a function of height, the presence of radon can be derived and characterized. Chapter 5, section 5.4 of van der Veeke (2023) describes the implementation of UAV-borne radon calibration flights.

For conventional airborne measurements, flights over a calibration range at several heights should be done to estimate the attenuation of gamma-ray as a function of altitude. These height measurements are typically flown in the range of 60 to 240 m, and the purpose is to verify the plywood calibrations (International Atomic Energy Agency, 1991). After initial flights at several heights, daily flights along this reference line are advised to monitor changes in the spectrometer response over time and monitor the effects of moisture in the ground. These flights require access to a suitable calibration range where the elemental concentrations are known (Seligman, 1992). Although these flights are still part of the guidelines for airborne radioelement mapping (Nicolet and Erdi-Krausz, 2003), such flights have several caveats. Firstly, such a calibration range should be available in the vicinity of the measurement. Secondly, the measurement platform has to fly the exact same

path every time. This is difficult, and there will always be variations in the spatial position, height and speed of the measurement platform. Thirdly, the measurement is affected not only by the detector response, but also by the soil moisture.

Because of the caveats with conventional airborne measurements, a new procedure is proposed for UAV-borne measurements. This procedure makes use of the characteristic that most UAVs possess: the possibility to locate and hover at a static position.

a) If the detector has been calibrated using Monte-Carlo simulation and height corrections have been implemented by the procedure described in Chapter 3 of van der Veeke (2023) or van der Veeke et al. (2021a), no height calibration measurements are needed.

Alternatively, if the calibration is done on calibration pads and the plywood model for height corrections is used, static measurements should be done at several heights to verify the change in spectral shape and intensity. First, the maximum survey height of the measurement platform should be determined. Secondly, an area homogenous in radionuclide concentrations with the extent of the 95 % footprint at the maximum height should be identified. Several measurements should be done in the range of zero to the maximum measurement height. At each measurement height, the UAV should hover for the time needed so that the statistical uncertainty of this calibration measurement does not significantly influence the radionuclide analysis of the survey. The required uncertainty of the measurement is defined in step 1 (section 0 in this publication), and the number of counts that need to be collected in an energy interval depends on the chosen analysis method. The values for stationary height should be converted to effective height by including the atmospheric temperature and pressure, and an estimate of the soil moisture in the area should be made.

b) The flight over a calibration range to characterize the response of the detector is replaced by the resolution test described in the next section.

c) In a multiday survey in which the soil moisture could significantly change over the measurement period, a calibration point should be selected. At the start of each

survey day, a measurement at the survey height should be done at this point. Similar to the height measurements, the UAV should hover for the time needed to acquire radionuclide concentrations with an individual uncertainty smaller than the minimum defined in step 1 (section 0 in this publication). If a significant difference in the measured count rate or concentration of the calibration point is detected, the resulting data should be interpreted by taking this difference into account, or the collected data can be scaled by using the ratio between the values measured at the calibration point. When scaling the data, the assumption is made that the change in count rate due to soil moisture is the same throughout the survey area. Because this is difficult to verify, it is advised that a difference in soil moisture measurements is not used to scale the collected data but taken into account when interpreting the data.

Implementing all the calibration requirements described in this section leads to a fully characterized spectrometer that can reliably and accurately derive the radionuclide concentrations from the recorded gamma-ray spectra. Depending on the intensity of use of the system and the crystal type, these calibration flights have to be done at least every three to five years and remain valid within this time as long as the daily checks, described in the next sections, remain within the predefined range of acceptable values.

1.4 Survey: quality control before and during the survey

The UAV-borne gamma-ray survey can be executed if all the steps and prerequisites from the previous sections have been fulfilled. The original guidelines for radioelement mapping list several checks that evaluate the quality and stability of the recorded spectra. This section results from a re-evaluation of the conventional assessments and extends this with geostatistical quality verification checks. The latter is possible due to the next generation of gamma-ray spectrometer systems that record the data and do a preliminary radionuclide analysis and synchronize the spectral data to positional data. These *smart* measurement systems allow real-time inspection of the collected data and enable the survey operator to adjust the survey plan while taking measurements. The aim of these data quality checks is to maximize the information captured during the survey.

1.4.1 Step: 4.1 Prior to the measurement: verify stable atmospheric conditions

The influence of radon in the measurement should be minimized. Potential atmospheric influences are listed in Chapter 5 of van der Veeke (2023), and the review of information available in the literature presented in this publication concludes with the following guidelines for the atmospheric conditions during the survey (Chapter 5, section 5.2.3.1 of van der Veeke (2023)):

It is recommended that a gamma-ray survey takes place between 11 AM and 5 PM, not within three hours after rainfall. In that case, when there is some wind, preferable cloudy, and the weather remains fair, a homogenous radon concentration can be assumed to extend up to 1000 m around the measurement in both the horizontal and vertical plane.

This advice maximizes the probability of a low and homogenous radon concentration throughout the survey and makes it possible to apply a correction for the contribution of radon decay in the atmosphere to the recorded data. The atmospheric conditions during the survey should be monitored to remain as prescribed.

1.4.2 Step: 4.2 Conventional checks

The conventional checks described in Nicolet and Erdi-Krausz (2003) focus on the quality of the collected spectra. Daily tests with a thorium source, checking the resolution of the 2.61 MeV thorium peak and monitoring the spectral stability are prescribed to ensure that the detector characteristics do not change over time.

Daily tests with a thorium source placed in a fixed relative position to the spectrometer are implemented to ensure the sensitivity of the system. The background-corrected thorium count rate must be within 5 % of the average of the recent thorium source tests (Nicolet and Erdi-Krausz, 2003). For an accurate reading, the thorium source always has to be positioned at the exact same position with respect to the spectrometer; otherwise, geometric differences can introduce a count rate difference.

Checking the resolution of the thorium peak: The highest peak present in the spectrum when measuring naturally occurring radionuclides should be used to verify the resolution of the spectrometer. This verification is done by accumulating

sufficient data so that the 2.61 MeV peak from the decay of ^{208}Tl is well defined in the measurement. From this well-defined peak, the FWHM can be calculated and represented as the resolution (%). The resolution of this thorium peak should be within 5 % of the average of the recent resolution readings.

Monitoring spectral stability: if the system uses a live energy calibration (Section 1.5.3 in this publication), the spectral stability should be verified. This verification is to ensure that the whole spectrum is included in the measurement and the peaks are at the correct energy position. In case post-processing stabilization is used, it should be verified that the raw spectrum collects the full 0–3 MeV energy range and that the 2.61 MeV thorium peak is located at 80 % of the spectrum channels (e.g. at channel 400 for a 512 channel MCA) to allow a small temperature drift during the survey.

1.4.3 Step: 4.3 Checks during the survey

If all the checks have been done and the results pass the requirements, the survey along the flight path determined in section 1.2 of these guidelines can be executed. Additional data checks can be implemented during the collection of spectral data:

The latest generation of gamma-ray spectrometers (e.g. Medusa spectrometers (Medusa Radiometrics, 2021)) contains an embedded microprocessor that autonomously collects spectral and auxiliary sensor data. The data from all the auxiliary sensors are merged with the analysed spectra and result in preliminary geotagged radionuclide concentrations. Although not all analysis steps described in the next section (post-processing) are currently implemented in the onboard analysis, the real-time radionuclide concentrations enable a whole new range of data quality verifications while the survey is still ongoing. The recommendations below are based on the current capabilities of gamma-ray spectrometers, and considering the novelty of these features, it is expected that the real-time analysis possibilities are subject to further improvement in the coming years.

The direct availability of radiometric data with a spatial position leads to the possibility of checking:

The spatial radionuclide distribution: in the survey design, the radionuclide concentration of the area is estimated. The detector size and survey parameters such

as flying height and speed are selected based on these estimated concentrations. It should be checked that the measured concentrations are in the same range as the estimated concentrations used to develop the survey plan.

The spatial uncertainty in radionuclide distribution: closely related to the radionuclide distribution is the uncertainty per measured point. Plotting the uncertainty distribution makes it clear what parts of the survey have sufficiently been measured and what areas should be revisited. This check is to ensure that the concentrations measured in each area have an uncertainty within the predetermined limits.

All the above checks facilitate the adjustment of survey parameters during the execution of the survey. If the preliminary results show that a particular area has a higher or lower radionuclide concentration than expected, the flying speed, height and measurement frequency can be adjusted accordingly. The adjustment of survey parameters optimises the time used to survey the area.

Adjusting the survey parameters should be done with good knowledge of the impact of the various survey parameters on the resulting data. Altering the measurement height changes the footprint, and modifying the movement speed changes the elongation of this footprint. Therefore, altering these parameters should be done with care and, where possible, compensated by changing multiple parameters. E.g., when decreasing the measurement height, the integration time or movement speed and line separation should be adjusted to prevent elongation of the footprint and to ensure a measurement frequency above the Nyquist-Shannon frequency.

1.5 Post survey: Data processing

The main goal of a gamma-ray survey is to estimate the absolute radionuclide concentrations in the survey area, which is done through the data processing steps described in this section. Several corrections have to be applied to the recorded gamma-ray spectra to obtain absolute concentrations. Although this section is titled 'post survey', recently developed 'smart' measurement systems have already implemented some of the steps described below. The expectation is that with the ongoing development of the hard- and software of modern gamma-ray spectrometer, more data processing steps will be automated and embedded in the spectrometer.

The continued improvement of gamma-ray spectrometry systems' autonomous data processing capabilities makes them easier to use because detailed spectral processing knowledge is not needed to work with the system. However, for non-standard applications, the automated data processing might not be adequate and may result in incorrect radionuclide concentrations. Therefore, this section describes all the processing steps needed to go from raw spectral data to radionuclide concentrations. Some data processing steps use the entire dataset collected in the survey to correct the individual spectra and are less suited to be applied in real-time. This section concludes with a discussion on the outlook for automated spectral data processing.

1.5.1 Step 5.1: pre-processing

Recorded data from all sensors need to be merged. All the sensor recordings, such as the GPS, pressure, temperature and humidity sensors, need to be synchronized to the spectral readings. If the recorded timestamps do not exactly match, this can be done by estimating the values through interpolation. Some sensor readings, such as the LiDAR, might benefit from averaging to smooth out rapid changes. The pre-processing step should also include a first check on the recorded spectral data, check for completeness of the dataset. The recorded heights should be converted to standard temperature and pressure (STP) height (h_{stp}), a parameter that corrects for atmospheric pressure and temperature (International Atomic Energy Agency, 1991):

$$h_{stp} = \frac{273.15 * P * h_{obs}}{(T + 273.15) * (101.325)} \quad (1.2)$$

in which P is the measured pressure (kPa) at height h_{obs} , h_{obs} is the observed height above ground level (m) and T is the observed temperature (°C).

1.5.2 Step 5.2: live-time correction

MCAs have, after an input signal is received, a dead time during which the device cannot accept new input due to the time needed for processing the current signal. The overall dead time is in first-order proportional to the count rate. In geophysical gamma-ray measurements, dead time is usually small, but in cases when an anomaly with very high activity is measured, it can significantly increase. A typical MCA will report the time actually measured (live-time (t_{lt})), the time passed during the

measurement (real-time (t_{rt})) and the resulting time that no measurement was taking place (dead-time (t_{dt})), which is usually reported as a percentage. The live-time is the time that should be used in the radionuclide analysis described in the subsequent sections.

1.5.3 Step 5.3: Energy calibration

Most scintillation crystals have a temperature-dependent light output, and due to this, some systems suffer from drift in the photomultiplier output. This drift will result in a temperature-dependent energy shift of the spectrum. There are two approaches to compensate for this drift:

Live correction: Continuously updating the high voltage or gain so that the peaks stay at the same positions. This continuous update can either be done by characterizing the temperature-dependent response of the crystal and implementing this correction based on this curve or by implementing a feedback circuit that monitors the known peaks present in the spectrum and adjusts the high voltage or gain when these peaks appear at the wrong energy. Note that this process needs a certain number of counts to determine the spectral shape which results in a lag in the adjustment of the peak positions.

Post-processing correction: This correction redistributes the energy bin contents of the spectrum during post-processing based on the positions of the known peaks, similarly to the feedback circuit in the live corrections (Hendriks et al., 2001; Medusa Radiometrics, 2012).

Both methods have their limitations. A temperature curve assumes that the temperature of the crystal is homogenous and equal to the temperature measured by the temperature sensor. The live feedback circuit implements a non-reversible change, resulting in non-usable spectra when the shift is sufficiently large so that peaks are wrongly identified. For instance, in the extreme situation, that the 1.46 MeV peak (^{40}K) is wrongfully detected as the 2.61 MeV (^{208}Tl , part of the ^{232}Th decay chain). This erroneous detection will cause the high voltage or gain to change and shift the spectrum so that all the counts above the 1.46 MeV peak will fall outside of the monitored channels. The post-processing redistribution of the channel contents allows the manual adjustment in the case of wrongfully detected peaks since no information was lost permanently. However, redistributing the channel contents during post-processing can result in fractional counts being distributed over

multiple channels, influencing the assumption of individual events per channel on which the Poisson statistics for uncertainty estimation are based. Additionally, the post-processing redistribution requires the setting of the spectrometer such that temperature drift will never shift the 2.61 MeV peak out of the recorded energy range.

The gamma-ray spectrometer manufacturer usually prescribes the energy calibration method because the live energy corrections are hardware-based. If this hardware has not been implemented, the correction can only be done in post-processing.

1.5.4 Step 5.4: Spectral smoothing (optional)

The two spectral smoothing techniques commonly implemented in airborne gamma-ray surveys are Noise Adjusted Singular Value Decomposition (NASVD) and the Maximum Noise Fraction (MNF) method (Dickson and Taylor, 2000; Green et al., 1988; Jens Hovgaard, 1979; Lee et al., 1990; Mairing and Smethurst, 2005; Minty and McFadden, 1998). Both methods are essentially principal component decomposition methods in which the lower-order components are kept and the higher-order components, containing mostly noise, are discarded. The difference between the methods is how they handle the noise present in the spectra, and it has been shown that both methods produce almost identical results. (Minty and Hovgaard, 2002).

The goal of the smoothing techniques is to decrease the uncertainty of the resulting radionuclide concentrations, but both methods should be applied with caution because:

- a) The smoothing methods are usually applied to large datasets over large regions in which successive readings are very similar. The latter is a reasonable assumption in geophysical surveys if no sudden variations are expected, but this is not always the case.
- b) Both smoothing methods do not accommodate for height-related changes in spectral shape in the data used to calculate the smoothing.

Thus, based on b), smoothing should only be applied to data measured at the same

height⁴, and due to a), small anomalies may not be well represented in the higher-order components.

Although, until today, this technique is not widely used in UAV-borne surveys, these techniques are included in these guidelines because of their proven enhancement of air-borne collected spectral data. However, considering the different scale of UAV-borne surveys and the known height dependence of the spectral shape, it is advised to apply these techniques with caution and only when the survey has been collected in constant height mode and contains no anomalies.

1.5.5 Step 5.5: Cosmic and radon background corrections

The cosmic spectrum is scaled by using the contents of the cosmic channel, and the result is subtracted from the measurement. The presence and contribution of atmospheric radon is established as described in Chapter 5 of van der Veeke (2023). The radon contribution should be subtracted from the measured spectra by using the methodology presented in Chapter 5, section 5.4 of van der Veeke (2023). If the survey was flown over multiple days in which the radon concentration was established, this radon identification and correction should be applied to each day independently.

1.5.6 Step 5.6: Reduction to elemental concentrations

The spectra that result after the corrections applied in the previous steps can now be used to derive the radionuclide concentrations in the ground. Two commonly used methods to extract the concentrations from the spectra are the Windows Analysis (WA) method and the Full Spectrum Analysis (FSA) method. Both methods need a calibration in which the response of the detector to the radionuclide concentrations is established. The WA method uses this information in the form of stripping ratios, and the FSA method uses this in the form of standard spectra; both represent the response of the spectrometer to 1 Bq kg⁻¹ of ground concentration. The difference lies in the part of the spectrum that is used for the analysis. The calibration for both methods is described in section 1.3 of this publication. The full description of the WA method (Nicolet and Erdi-Krausz, 2003) and FSA (Dickson, 1980; Hendriks et al.,

⁴ Constant height: the separation between the ground and the detector should be kept constant.

2001) method can be found in the literature; below is a short summary of the principles which are schematically represented in Fig. 1.5.

The WA method identifies three energy windows in which prominent peaks of ^{40}K , ^{238}U and ^{232}Th are located (defined in Table 1.2). The number of counts in each window for each element for 1 Bq kg^{-1} can be extracted from the detector calibration, which are called the sensitivities of a detector. A measured spectrum gives the counts in each of the three energy windows. The sensitivities and counts for all three windows give three equations to resolve three radionuclide concentrations and can be rewritten in matrix form. By diagonalizing the matrix and taking the square roots of the elements, the uncertainty is calculated. Counts in the 2.61 MeV peak (due to ^{208}Tl , part of the ^{232}Th decay chain) can only be attributed to ^{232}Th because ^{40}K and ^{238}U do not emit gamma-rays in this energy range. Similarly, counts in the 1.76 MeV window can be attributed to both ^{232}Th and ^{238}U and analogously, counts in the 1.46 MeV window can be attributed to all three radionuclides.

The WA method's major caveat in this application of the analysis of geophysical gamma-ray spectra is that uncertainty in the determination of the ^{232}Th concentration propagates in the uncertainty of ^{238}U and ^{40}K , and the uncertainty of ^{238}U additionally increases the uncertainty in ^{40}K . The uncertainty in the concentrations decreases when a larger number of counts, related to the quantity that is measured, is used in the analysis. The WA method only uses the counts captured in the selected energy windows and discards the counts collected outside these windows. Consequently, as part of the information present in the spectrum is not used, this will increase the uncertainties.

FSA fits the measured spectra with calibrated standard spectra that represent the detector's response to a pure source of 1 Bq kg^{-1} of ^{40}K , ^{238}U or ^{232}Th (Hendriks et al., 2001). The radionuclide concentrations are the normalization factors of the standard spectra in the best fit of the measured spectrum. FSA uses the entire spectrum to determine the nuclide concentrations, and the larger number of counts included in the analysis interval, compared to the WA method, can lead to lower uncertainties if the individual spectra are sufficiently different. The latter is the case in geophysical gamma-ray measurement. The limitation of the FSA method is that the standard spectra have to be available. An advantage of FSA is that any number of standard spectra can be added to the analysis, for instance, ^{137}Cs . The only requirement is that

the standard spectra are sufficiently different so that the radionuclide extraction process can separate the individual contributions. Similar to the WA method, as the spectra are not orthogonal, the off-diagonal elements of the covariance matrix will be non-zero, and the uncertainties in the concentrations will be interdependent.

Both methods need to correct for effective measurement height (h_{stp}), calculated in step 1. FSA should use spectra simulated at each height as described in Chapter 3 of van der Veeke (2023) or van der Veeke et al. (2021a) to accommodate the spectral shape changes as a function of height. The same argument holds for determining the stripping ratios of the WA methods. An alternative to the use of Monte-Carlo simulations to determine the stripping ratios and standard spectra at height is using the plywood method described in section 1.3 of this publication. The height corrected standard spectra and stripping ratios should be used to derive the elemental radionuclide concentrations in the ground.

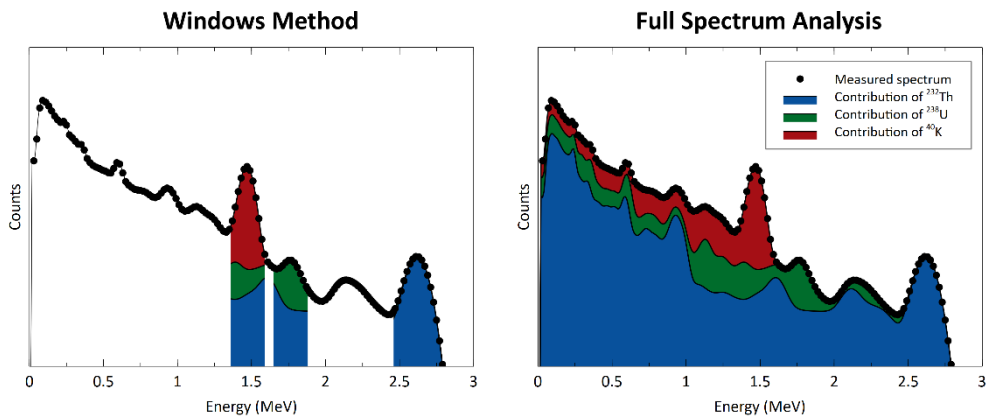


Fig. 1.5. Schematic representation of the WA and FSA methods. The contributions of ^{232}Th (blue), ^{238}U (green) and ^{40}K (red) are shown. The potassium peak has a contribution of uranium and thorium, and the uranium peak has a contribution of thorium. WA analysis only uses the counts in the specified windows, whereas the FSA uses counts in the whole spectrum.

1.5.7 Step 5.7: Verification of the tie-lines

After the analysis in which environmental and geometry corrections have been applied, the radionuclide concentrations of the tie-lines should match the concentrations of the grid measurements. Due to the stochastic nature of radioactive decay, an exact match is unlikely, but the measurements should agree within a confidence limit of 95 % when using a Z-test, taking their individual uncertainty into

account. If this is not the case, the measurements and corrections should be re-evaluated. Minor differences in the radionuclide concentration values can be attributed to a different footprint of the tie-line measurements compared or in the case of surveys flown on different days due to soil moisture in the ground. The magnitude of these effects can be estimated (footprint: Chapter 3 of van der Veeke (2023) or van der Veeke et al. (2021a), soil moisture: Chapter 6 of van der Veeke (2023)) and compared to the differences in radionuclide concentrations for the tie- and grid-lines. If this still cannot explain the differences in radionuclide concentrations, this may indicate equipment failure has occurred, e.g. a GPS offset or a malfunctioning MCA.

1.5.8 Step 5.8: Interpolation and interpretation

The resulting spatially distributed radionuclide concentrations represent the radionuclide concentrations in the ground at their measured position. Usually, these results are interpolated to create maps, as shown in Fig. 1.6. Multiple specialized Geographic Information System (GIS) software tools are available for this map-making process, and the exact implementation of this interpolation process is out of the scope of these guidelines. However, these maps are often the final product of a survey, and their interpretations may be used for decisions or advice that have far-reaching implications. Therefore, we list some points of attention and guidelines that may assist in interpolating and interpreting radionuclide maps.

a. Choice of interpolation method: the value of the estimated radionuclide concentration in between the measured points depends on the used interpolation methods. This difference mainly lies in the amount of data used to interpolate at each point and the underlying assumptions of the variation in the data. Therefore, the interpolation methods should be chosen based on the expected underlying spatial variation in the data.

Good results have been achieved for mapping naturally occurring radioactivity by using the variogram in combination with Kriging (Andreasen et al., 2021; Desnoyers and Dubot, 2011) or by using inverse distance weighting (Habib et al., 2019). Using the variogram has the added benefit of assessing the spatial variance in the data and the ability to compare this spatial variance to the uncertainty per data point.

b. Reporting of uncertainty: as crucial as the reported values of the radionuclide concentrations is their associated uncertainty. Without these uncertainties, it is impossible to effectively assess the distribution and estimate the significance of the found concentration variations. Radionuclide concentrations have an inherent uncertainty due to the stochastic nature of the processes involved: radioactive decay, the interaction of gamma-rays with the environment and in the detector, and the translation of the energy deposit to an electrical signal. The standard mathematical uncertainty propagating methods should be adhered when applying the correction described in this post-processing section. Suppose this uncertainty for each data point has a similar magnitude or is larger than the spatial variation in radionuclide concentration. In that case, the conclusion of the measurement can only be that there is no statistically significant variation measured (within the limits of the uncertainty). Besides the inherent uncertainty associated with the radioactive decay process, there will also be uncertainty due to interpolation. The possibility and quality of interpolation uncertainty maps are dependent on the choice of interpolation software but should always be part of the assessment of the resulting maps.

c. Choice of colour scale: it should be realized that different colours have different psychological connotations. Commonly green is associated with good, and red is associated with bad. Furthermore, the human eye's response is not the same for each colour (Wandell and Thomas, 1997). Therefore, the choice of colour scale will impact the perceived interpretation of the map. A good colour scale is perceptually uniform, i.e. the distance between two colours as perceived by the human eye is proportional to the distance between two data points. Furthermore, a good scale requires that the visual interpretation is a proportional reflection of the actual variation. At the same time, the colours on the map should appropriately highlight areas of interest. A single hue colour scale could be used to overcome cultural colour interpretations (e.g. green is good, red is bad). Tools are available that help to select a good colour scale for the intended application (Harrower and Brewer, 2003). For radiometric measurements, a perceptually uniform single-hue colour space for ^{40}K , ^{238}U and ^{232}Th can be used, as shown in Fig. 1.6 or in Chapter 4 of van der Veeke (2023) or van der Veeke et al. (2021b).

d. Interpretation: gamma-ray measurements aim to map the radionuclide concentration in the ground, and the measurement height significantly limits the spatial resolution because spatial variation within the footprint of the measurement cannot be fully captured. This concept is outlined in section 1.2 of this publication, which is based on Chapter 3 of van der Veeke (2023) or van der Veeke et al. (2021a). A comparison of ground and UAV-borne measurements has verified that concentrations derived from surveys with a larger footprint will regress to the mean value of the radionuclide concentration within the footprint (Chapter 4 of van der Veeke (2023) or van der Veeke et al (2021b)). In monitoring naturally occurring radioactivity, the concentration will most likely vary gradually, and therefore this footprint averaging is less of a problem than when searching for point sources. Nevertheless, this regression to the mean effect should be realized when interpreting the resulting radionuclide maps: radionuclide concentrations of hot- and cold-spots will appear closer to the mean value than is the case in reality.

1.5.9 Step 5.9: Additional data processing methods (optional)

When appropriate, additional methods that can help in the deconvolution of the radioelement concentrations in the ground can be applied. Examples of these methods can be found in the literature, e.g. the inclusion of the 3D variation in terrain height and accounting for the directional sensitivity of the gamma-ray spectrometer (Minty and Brodie, 2016), spatial deconvolution for finding hotspots (Sinclair and Fortin, 2019) or using horizontal gradients to improve the spatial resolution of the detector (Beamish, 2016).

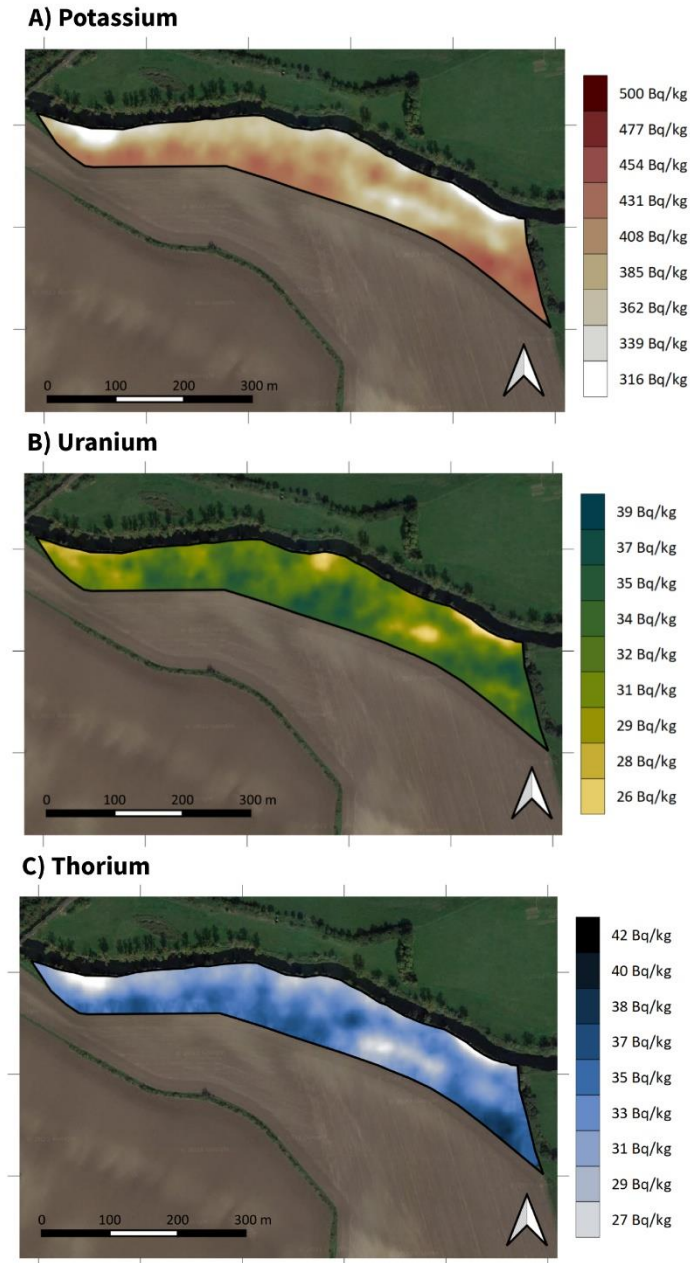


Fig. 1.6. Typical interpolated maps for the radionuclides ^{40}K , ^{238}U and ^{232}Th from a UAV-borne survey from a field with limited spatial variability. Average 1σ uncertainty for the ^{40}K , ^{238}U and ^{232}Th plots are 46, 7.0 and 4.9 Bq kg $^{-1}$ per measurement point.

References

- Aab, A. *et al.* (The Pierre Auger Collaboration), 2020. Measurement of the cosmic-ray energy spectrum above 2.5×10^{18} eV using the Pierre Auger Observatory. *Physical Review Letters* 125, 121106.
<https://doi.org/10.1103/PhysRevLett.125.121106>
- Ademila, O., Akingboye, A.S., Ojamomi, A.I., 2018. Radiometric survey in geological mapping of basement complex area of parts of Southwestern Nigeria. *Vietnam Journal of Earth Sciences* 40, 288–298.
<https://doi.org/10.15625/0866-7187/40/3/12619>
- Andreasen, M., Limburg, H., van der Veeke, S., Looms, M.C., 2021. Forest plot soil moisture estimation using the cosmic-ray neutron (CRN) method and gamma-ray spectrometry (GRS), in: AGU Fall Meeting 2021. pp. H55C-0769.
- Beamish, D., 2016. Enhancing the resolution of airborne gamma-ray data using horizontal gradients. *Journal of Applied Geophysics* 132, 75–86.
<https://doi.org/10.1016/j.jappgeo.2016.07.006>
- Billings, S.D., Minty, B.R., Newsam, G.N., 2003. Deconvolution and spatial resolution of airborne gamma-ray surveys. *Geophysics* 68, 1257–1266.
<https://doi.org/10.1190/1.1598118>
- Bird, A.J., Carter, T., Dean, A.J., Ramsden, D., Swinyard, B.M., 1993. The optimisation of small CsI (Tl) gamma-ray detectors. *IEEE transactions on nuclear science* 40, 395–399. <https://doi.org/10.1109/23.256587>
- Burrough, P.A., McDonnell, R.A., Lloyd, C.D., 2015. Principles of geographical information systems. Oxford university press.
- Cabreira, T.M., Brisolará, L.B., Ferreira Paulo, R., 2019. Survey on coverage path planning with unmanned aerial vehicles, Drones.
<https://doi.org/10.3390/drones3010004>
- Cheng, H., Sun, B.-H., Zhu, L.-H., Li, T.-X., Li, G.-S., Li, C.-B., Wu, X.-G., Zheng, Y., 2020. Intrinsic background radiation of LaBr₃(Ce) detector via coincidence measurements and simulations. *Nuclear Science and Techniques* 31, 99. <https://doi.org/10.1007/s41365-020-00812-8>
- De Wegenscanners BV, 2021. De Wegenscanners BV [WWW Document]. URL <https://dewegenscanners.nl/> (accessed 11.25.21).
- Desnoyers, Y., Dubot, D., 2011. Geostatistical methodology for waste optimization of contaminated premises, in: International Conference on Radioactive Waste Management and Environmental Remediation. pp. 239–244.
<https://doi.org/10.1115/ICEM2011-59344>
- Dickson, B., Taylor, G., 2000. Maximum noise fraction method reveals detail in aerial gamma-ray surveys. *Exploration Geophysics* 31, 73–77.
<https://doi.org/10.1071/EG00073>
- Dickson, B.H., 1980. Analytic methods for multichannel airborne radiometrics. University of Toronto.
- Egmond, F.M. Van, Veeke, S. Van Der, Knotters, M., Koomans, R.L., Limburg, J., 2018. Mapping soil texture with a gamma-ray spectrometer : comparison

- between UAV and proximal measurements and traditional sampling. WOt-technical report 137, 58p. <https://doi.org/http://edepot.wur.nl/466037>
- Förstner, U., Hollert, H., Brinkmann, M., Eichbaum, K., Weber, R., Salomons, W., 2016. Dioxin in the Elbe river basin: policy and science under the water framework directive 2000–2015 and toward 2021 Background. *Environ Sci Eur* 28. <https://doi.org/10.1186/s12302-016-0075-8>
- Gilmore, G., 2008. Practical gamma-ray spectroscopy. John Wiley & Sons. <https://doi.org/10.1002/9780470861981>
- Grasty, R.L., Minty, B.R.S., 1995. A Guide to the Technical Specifications for Airborne Gamma-Ray Surveys. Australian Geological Survey Organisation.
- Grasty, R.L., Shives, R.B.K., 1997. Applications of gamma ray spectrometry to mineral exploration and geological mapping, in: Workshop Presented at Exploration.
- Green, A.A., Berman, M., Switzer, P., Craig, M.D., 1988. A Transformation for Ordering Multispectral Data in Terms of Image Quality with Implications for Noise Removal. *IEEE Transactions on Geoscience and Remote Sensing* 26, 65–74. <https://doi.org/10.1109/36.3001>
- Habib, M.A., Basuki, T., Miyashita, S., Bekelesi, W., Nakashima, S., Phoungthong, K., Khan, R., Rashid, M.B., Islam, A.R.M.T., Techato, K., 2019. Distribution of naturally occurring radionuclides in soil around a coal-based power plant and their potential radiological risk assessment. *Radiochimica Acta* 107, 243–259. <https://doi.org/10.1515/ract-2018-3044>
- Harrower, M., Brewer, C.A., 2003. ColorBrewer.org: An online tool for selecting colour schemes for maps. *Cartographic Journal* 40, 27–37. <https://doi.org/10.1179/000870403235002042>
- Hebinck, K., Middelkoop, H., Diepen, N. van, der Graaf, E.R., De Meijer, R.J., 2007. Radiometric fingerprinting of fluvial sediments in the Rhine-Meuse delta, the Netherlands – a feasibility test. *Netherlands Journal of Geosciences* 86, 229–240. <https://doi.org/10.1017/S0016774600077829>
- Hendriks, P.H.G.M., Limburg, J., De Meijer, R.J., 2001. Full-spectrum analysis of natural γ -ray spectra. *Journal of Environmental Radioactivity* 53, 365–380. [https://doi.org/10.1016/S0265-931X\(00\)00142-9](https://doi.org/10.1016/S0265-931X(00)00142-9)
- International Atomic Energy Agency, 1991. Airborne gamma ray spectrometer surveying., technical reports series no. 323. International Atomic Energy Agency, Vienna.
- Jakovlevs, O., Pchelintsev, A., Malgin, V., Sokolov, A., Gostilo, V., 2018. Development of miniaturized HPGe spectrometers for unmanned aerial vehicles. *Journal of Instrumentation* 13. <https://doi.org/10.1088/1748-0221/13/06/T06006>
- Jens Hovgaard, 1979. A new processing technique for airborne gamma-ray data, in: Proceedings from the Sixth Topical Meeting on Emergency Preparedness & Response. American Nuclear Society, United States.
- Knotters, M., 2015. De waarde van een gedetailleerde bodemkaart van een waterwingebied. *Stromingen: vakblad voor hydrologen* 21, 29–41.
- Koomans, R., der Veeke, V., Jacobs, P., Limburg, H., 2019. Mapping Sediment Contamination with a Gamma-Ray Spectrometer, Underwater and on Land,

- in: 25th European Meeting of Environmental and Engineering Geophysics. pp. 1–5.
- Koomans, R., Limburg, H., 2020. Drone-borne gamma-ray spectrometry – a dream come true! *Fast times* 25, 70–76.
- Koomans, R.L., 2000. *Sand in motion: effects of density and grain size*. University of Groningen, The Netherlands.
- Koomans, R.L., van der Wal, P., Kamsma, T.P.J., 2014. A Geophysical Technique for the Verification and Quantification of Zinc Slag in Roads, in: *Near Surface 2009 - 15th EAGE European Meeting of Environmental and Engineering Geophysics*. <https://doi.org/10.3997/2214-4609.20147047>
- Lee, C., Kim, H.R., 2019. Optimizing UAV-based radiation sensor systems for aerial surveys. *Journal of Environmental Radioactivity* 204, 76–85. <https://doi.org/10.1016/j.jenvrad.2019.04.002>
- Lee, J.B., Woodyatt, A.S., Berman, M., 1990. Enhancement of High Spectral Resolution Remote-Sensing Data by a Noise-Adjusted Principal Components Transform. *IEEE Transactions on Geoscience and Remote Sensing* 28, 295–304. <https://doi.org/10.1109/36.54356>
- Letaw, J.R., Share, G.H., Kinzer, R.L., Silberberg, R., Chupp, E.L., Forrest, D.J., Rieger, E., 1989. Satellite observation of atmospheric nuclear gamma radiation. *Journal of geophysical research* 94, 1211–1221. <https://doi.org/10.1029/JA094IA02P01211>
- Liu, B., Duan, X., Yan, L., 2018. A Novel Bayesian Method for Calculating Circular Error Probability with Systematic-Biased Prior Information. *Mathematical Problems in Engineering* 2018, 5930109. <https://doi.org/10.1155/2018/5930109>
- Liu, Y., Zhou, W., Gao, B., Zheng, Z., Chen, G., Wei, Q., He, Y., 2021. Determination of radionuclide concentration and radiological hazard in soil and water near the uranium tailings reservoir in China. *Environmental Pollutants and Bioavailability* 33, 174–183. <https://doi.org/10.1080/26395940.2021.1951123>
- Loeborg, L., 1984. *Design and use of concrete pads for the calibration of radiometric survey instrumentation*.
- MacFarlane, J.W., Payton, O.D., Keatley, A.C., Scott, G.P.T., Pullin, H., Crane, R.A., Smilion, M., Popescu, I., Curlea, V., Scott, T.B., 2014. Lightweight aerial vehicles for monitoring, assessment and mapping of radiation anomalies. *Journal of Environmental Radioactivity*. <https://doi.org/10.1016/j.jenvrad.2014.05.008>
- Martin, P.G., Kwong, S., Smith, N.T., Yamashiki, Y., Payton, O.D., Russell-Pavier, F.S., Fardoulis, J.S., Richards, D.A., Scott, T.B., 2016a. 3D unmanned aerial vehicle radiation mapping for assessing contaminant distribution and mobility. *International Journal of Applied Earth Observation and Geoinformation* 52, 12–19. <https://doi.org/10.1016/j.jag.2016.05.007>
- Martin, P.G., Payton, O.D., Fardoulis, J.S., Richards, D.A., Scott, T.B., 2015. The use of unmanned aerial systems for the mapping of legacy uranium mines. *Journal of Environmental Radioactivity*. <https://doi.org/10.1016/j.jenvrad.2015.02.004>
- Martin, P.G., Payton, O.D., Fardoulis, J.S., Richards, D.A., Yamashiki, Y., Scott,

- T.B., 2016b. Low altitude unmanned aerial vehicle for characterising remediation effectiveness following the FDNPP accident. *Journal of Environmental Radioactivity* 151, 58–63.
<https://doi.org/10.1016/j.jenvrad.2015.09.007>
- Mauring, E., Smethurst, M.A., 2005. Reducing noise in radiometric multi-channel data using noise-adjusted singular value decomposition (NASVD) and maximum noise fraction (MNF). Geological survey of Norway NGU-rapport 2005.014.
- McKinney, G.W., Armstrong, H., James, M.R., Clem, J., Goldhagen, P., 2012. MCNP6 cosmic-source option. Los Alamos National Lab, United States.
- Medusa Radiometrics, 2021. MS-2000 product page [WWW Document]. URL <https://the.medusa.institute/pages/viewpage.action?pageId=3932225> (accessed 4.1.20).
- Medusa Radiometrics, 2012. Gamman User Manual.
- Medusa Radiometrics BV, 2020. Medusa Radiometrics BV [WWW Document]. URL <http://medusa-radiometrics.com> (accessed 12.9.19).
- Meijer, R. De, 1998. Heavy minerals: from Edelstein to Einstein. *Journal of Geochemical Exploration* 62, 81–103. [https://doi.org/10.1016/S0375-6742\(97\)00073-3](https://doi.org/10.1016/S0375-6742(97)00073-3)
- Minty, B., Brodie, R., 2016. The 3D inversion of airborne gamma-ray spectrometric data. *Exploration Geophysics*. <https://doi.org/10.1071/EG14110>
- Minty, B., Hovgaard, J., 2002. Reducing noise in gamma-ray spectrometry using spectral component analysis. *Exploration Geophysics* 33, 172–176.
<https://doi.org/10.1071/EG02172>
- Minty, B., McFadden, P., 1998. Improved NASVD smoothing of airborne gamma-ray spectra. *Exploration Geophysics*. <https://doi.org/10.1071/EG998516>
- Minty, B.R.S., 1998. Multichannel models for the estimation of radon background in airborne gamma-ray spectrometry. *Geophysics* 63, 1986–1996.
<https://doi.org/10.1190/1.1444492>
- Mochizuki, S., Kataoka, J., Tagawa, L., Iwamoto, Y., Okochi, H., Katsumi, N., Kinno, S., Arimoto, M., Maruhashi, T., Fujieda, K., Kurihara, T., Ohsuka, S., 2017. First demonstration of aerial gamma-ray imaging using drone for prompt radiation survey in Fukushima. *Journal of Instrumentation* 12, P11014--P11014. <https://doi.org/10.1088/1748-0221/12/11/p11014>
- Nicolet, J.P., Erdi-Krausz, G., 2003. Guidelines for radioelement mapping using gamma ray spectrometry data. International Atomic Energy Agency 179.
- Nilsson, J.M.C., Östlund, K., Söderberg, J., Mattsson, S., Rääf, C., 2014. Tests of HPGe- and scintillation-based backpack gamma-radiation survey systems. *Journal of Environmental Radioactivity*.
<https://doi.org/10.1016/j.jenvrad.2014.03.013>
- Park, S., Choi, Y., 2020. Applications of unmanned aerial vehicles in mining from exploration to reclamation: A review. *Minerals* 10, 663.
- Qassas, R.A.Y. El, Salaheldin, M., Assran, S.M.A., Fattah, T.A., Rashed, M.A., 2020. Airborne gamma-ray spectrometric data interpretation on Wadi Queih and Wadi Safaga area, Central Eastern Desert, Egypt. *NRIAG Journal of Astronomy and Geophysics* 9, 155–167.

- <https://doi.org/10.1080/20909977.2020.1728893>
- Radulescu, I., Rigollet, C., van der Graaf, E.R., de Meijer, R.J., 2007. Towards sub-centimetre resolution in bore-core logging. *Nuclear Instruments and Methods in Physics Research Section A: Accelerators, Spectrometers, Detectors and Associated Equipment* 580, 675–678.
<https://doi.org/10.1016/J.NIMA.2007.05.108>
- Šálek, O., Matolín, M., Gryc, L., 2018. Mapping of radiation anomalies using UAV mini-airborne gamma-ray spectrometry. *Journal of Environmental Radioactivity* 182, 101–107. <https://doi.org/10.1016/j.jenvrad.2017.11.033>
- Sanada, Y., Kondo, A., Sugita, T., Nishizawa, Y., Yuuki, Y., Ikeda, K., Shoji, Y., Torii, T., 2014. Radiation monitoring using an unmanned helicopter in the evacuation zone around the Fukushima Daiichi nuclear power plant. *Exploration Geophysics* 45, 3–7. <https://doi.org/10.1071/EG13004>
- Sanada, Y., Torii, T., 2015. Aerial radiation monitoring around the Fukushima Daiichi nuclear power plant using an unmanned helicopter. *Journal of Environmental Radioactivity* 139, 294–299.
<https://doi.org/10.1016/j.jenvrad.2014.06.027>
- Seligman, H., 1992. Airborne gamma ray spectrometer surveying, technical reports series no. 323: International Atomic Energy Agency, Vienna, 1991. 97 pp. Austrian Schillings 340.
- Shannon, C.E., 1949. Communication theory in the presence of noise. *Proceedings of the IRE* 37, 10–21.
- Share, G., 1999. Atmospheric gamma-ray lines produced by cosmic rays and solar energetic particles, in: 26th International Cosmic Ray Conference (ICRC26), Volume 7. p. 329.
- Share, G.H., Murphy, R.J., 2001. Atmospheric gamma rays from solar energetic particles and cosmic rays penetrating the magnetosphere. *Journal of Geophysical Research: Space Physics* 106, 77–92.
<https://doi.org/10.1029/2000JA002012>
- Sinclair, L.E., Fortin, R., 2019. Spatial deconvolution of aerial radiometric survey and its application to the fallout from a radiological dispersal device. *Journal of Environmental Radioactivity* 197, 39–47.
<https://doi.org/10.1016/J.JENVRAD.2018.10.014>
- Söderström, M., Eriksson, J., 2013. Gamma-ray spectrometry and geological maps as tools for cadmium risk assessment in arable soils. *Geoderma* 192, 323–334.
<https://doi.org/10.1016/j.geoderma.2012.07.014>
- Stenberg, A., Olsson, I.U., 1968. A low level gamma-counting apparatus. *Nuclear Instruments and Methods* 61, 125–133. [https://doi.org/10.1016/0029-554X\(68\)90533-8](https://doi.org/10.1016/0029-554X(68)90533-8)
- Taha, M., Mohamed, A., Latifa, ., Al-Naimi, S., Tochukwu, ., Chidiebere, ., Agoha, C., 2021. Geological mapping and mineral prospectivity using remote sensing and GIS in parts of Hamissana, Northeast Sudan 11, 1123–1138.
<https://doi.org/10.1007/s13202-021-01115-3>
- Tanczos, I., 1996. Selective transport phenomena in coastal sands. Rijksuniversiteit Groningen, The Netherlands.
- Trimble Inc., 2022. Trimble Inc. [WWW Document]. URL

- <https://geospatial.trimble.com/products-and-solutions/gnss-systems> (accessed 9.1.22).
- uBlox, 2021. uBlox ZED-F9P-02B Data sheet.
- UgCS, 2022.
- United Nations Scientific Committee, 2000. UNSCEAR 2000 Report to the General Assembly with Scientific Annexes, Vol. I: Sources, http://www.unscear.org/unscear/publications/2000_1.html.
- Van der Graaf, E.R., Koomans, R.L., Limburg, J., de Vries, K., 2007. In situ radiometric mapping as a proxy of sediment contamination: Assessment of the underlying geochemical and -physical principles. *Applied Radiation and Isotopes*. <https://doi.org/10.1016/j.apradiso.2006.11.004>
- Van der Graaf, E.R., Limburg, J., Koomans, R.L., Tijs, M., 2011. Monte Carlo based calibration of scintillation detectors for laboratory and in situ gamma ray measurements. *Journal of Environmental Radioactivity* 102, 270–282. <https://doi.org/10.1016/j.jenvrad.2010.12.001>
- Van der Klooster, E., Van Egmond, F.M., Sonneveld, M.P.W.W., 2011. Mapping soil clay contents in Dutch marine districts using gamma-ray spectrometry. *European Journal of Soil Science* 62, 743–753. <https://doi.org/10.1111/j.1365-2389.2011.01381.x>
- van der Veeke, S., 2023. UAV-borne radioelement mapping: towards a guideline and verification methods for geophysical field measurements. University of Groningen. <https://doi.org/10.33612/diss.261264637>
- van der Veeke, S., Limburg, J., Koomans, R.L., Söderström, M., de Waal, S.N., van der Graaf, E.R., 2021a. Footprint and height corrections for UAV-borne gamma-ray spectrometry studies. *Journal of Environmental Radioactivity* 231, 106545. <https://doi.org/10.1016/j.jenvrad.2021.106545>
- van der Veeke, S., Limburg, J., Koomans, R.L., Söderström, M., van der Graaf, E.R., 2021b. Optimizing gamma-ray spectrometers for UAV-borne surveys with geophysical applications. *Journal of Environmental Radioactivity* 237, 106717. <https://doi.org/10.1016/j.jenvrad.2021.106717>
- Venema, L.B., de Meijer, R.J., 2001. Natural radionuclides as tracers of the dispersal of dredge spoil dumped at sea. *Journal of environmental radioactivity* 55, 221–39.
- Vliegend.nl [WWW Document], 2022. URL <https://www.vliegend.nl/> (accessed 2.15.22).
- Wandell, B., Thomas, S., 1997. Foundations of vision. *Psychocritiques* 42.
- Ye, M., Gong, P., Wu, S., Li, Y., Zhou, C., Zhu, X., Tang, X., 2021. Lightweight SiPM-based CeBr₃ gamma-ray spectrometer for radiation-monitoring systems of small unmanned aerial vehicles. *Applied Radiation and Isotopes* 176, 109848. <https://doi.org/10.1016/J.APRADISO.2021.109848>
- Zhang, S., Liu, R., Zhao, T., 2018. Mapping radiation distribution on ground based on the measurement using an unmanned aerial vehicle. *Journal of Environmental Radioactivity* 193–194, 44–56. <https://doi.org/10.1016/j.jenvrad.2018.08.016>

List of abbreviations

CdZnTe	Cadmium zinc telluride
CRNS	Cosmic-Ray Neutron Sensor
CsI	Cesium Iodine (scintillation crystal material)
dBD	dry Bulk Density
DXTRAN	Deterministic Transport (MCNP algorithm)
fBD	field Bulk Density
FDR	Frequency-Domain Reflectometer
FSA	Full Spectrum Analysis
FWHM	Full Width at Half Maximum height
GNSS	Global Navigation Satellite System
GPS	Global Positioning System
gSMS	gamma Soil Moisture Sensor
HPGe	High Purity Germanium
IAEA	International Atomic Energy Agency
MCA	Multi Channel Analyser
MCNP	Monte-Carlo N-Particle code
MNF	Maximum Noise Fraction
MS-	Medusa Spectrometer
NaI	Sodium Iodine (scintillation crystal material)
NASVD	Noise Adjusted Singular Value Decomposition
NORM	Naturally Occurring Radioactive Material
PMT	Photo-Multiplier Tube
SD	Specific Density
SiPM	Silicon Photo-Multiplier
STP	Standard temperature and pressure
TDR	Time-Domain Reflectometer
UAV	Unmanned/Uncrewed Aerial Vehicle
WA	Windows Analysis

